Behavioral, Parameterized, and Broadband Modeling of Wired Interconnects with Internal Discontinuities

Behavioral, Parameterized and Broadband Modeling of Wired Interconnects with Internal Discontinuities

Stefano Grivet-Talocia, *Senior Member, IEEE*, Riccardo Trinchero, *Member, IEEE*

***Abstract*—We present a complete workflow for the extraction of behavioral reduced-order models of wired interconnect links, including an explicit dependence on geometrical or material parameters describing internal discontinuities that may affect the quality of signal transmission. Thanks to the adopted structure, the models are easily identified from sampled frequency responses at discrete points in the parameter space. Such responses are obtained from off-the-shelf full-wave solvers. A novel algorithm is used for checking and enforcing model stability and passivity, two fundamental requirements for reliably running stable transient simulations. Finally, an ad hoc procedure is devised to synthesize the models as parameterized circuit equivalents, compatible with any SPICE solver. Several examples illustrate and validate the workflow, confirming the suitability of proposed approach for what-if, parameter sweep, design centering and optimization through time-domain simulations, possibly including nonlinear devices and terminations.**

***Index Terms*—Macromodeling, parameterized modeling, behavioral modeling, transmission lines, high-speed interconnects, rational approximation, scattering, passivity, circuit equivalent, SPICE.**

I. Introduction and Motivation

Data transmission on wired interconnect links may be affected by several signal degradation effects. On one hand, metal and dielectric loss mechanisms give rise to unavoidable signal attenuation and dispersion. These effects are usually modeled through frequency-dependent dielectric permittivity, loss tangent, and conductor internal impedance [1], [2]. In time domain, such losses reduce signal amplitude and smooth switching fronts, thus practically limiting the bandwidth of the link. On the other hand, the particular geometry of the wired link, including both signal and return current routing, is very crucial for ensuring overall signal integrity. Whenever the differential nature of proagating current and its return is broken by some internal discontinuity, the latter may act as a frequency-selective filter that may cut-off important signal content and hinder safe data transmission [3]. Examples of internal discontinuities can be vertical via interconnects for routing through different PCB layers, or slots in the power/ground planes that provide return current path.

The above signal degradation effects require careful characterization and modeling since early design stages. Since the ultimate Signal Integrity verification is usually carried out in the time domain by checking pulse distortion or eye diagram opening, a highly desirable characterization of the link is a SPICE-compatible equivalent circuit, which can be run by Signal Integrity engineers using legacy circuit solvers [4], by embedding in the simulation deck linear or nonlinear termination networks. Unfortunately, a universal procedure that extracts a circuit equivalent of manageable size/complexity from arbitrary realistic irregular geometry and material specification is not available.

In this work, we propose a workflow for the extraction of compact, reduced-order behavioral circuit models of wired interconnect links, including an explicit dependence on suitably chosen parameters controlling shape/geometry of internal discontinuities. Section II provides a precise statement of the problem at hand. The workflow involves a set of preliminary full-wave analyses using any desired electromagnetic field solver for obtaining sampled frequency responses for few prescribed parameter configurations. This data is processed by a parameterized macromodeling engine [5], [6], which provides a closed-form approximation of the data in terms of rational functions of frequency and Chebychev polynomials of the parameter variables (Section III). Stability and passivity of the model is enforced using suitable constraints (Section V), and finally a parameterized SPICE netlist is exported (Section VI). To the best of Authors' knowledge, both the enforcement of uniform stability and passivity throughout the parameters space, and the proposed approach for parameterized SPICE equivalent extraction, are new contributions. The extraction of an initial parameterized macromodel from sampled responses is instead not new, more details can be found in [5], [7]–[9].

Various examples are used in Section VII to demonstrate the proposed workflow on template structures of wired links with internal discontinuities. Despite only few examples can be shown here due to limited space, the proposed approach is very general and applicable to any type of linear system whose frequency response depends smoothly on one or more parameters.

II. Problem statement

Let us consider the canonical structure depicted in Fig. 1, where a lumped RLC discontinuity is inserted in the middle of a uniform transmission line. This example will be used as a basic template to illustrate the proposed modeling workflow throughout this paper. In this template, we consider the capacitance C as a free parameter $C = \vartheta \in [0.1, 1]$ pF. The exact scattering matrix of the structure may thus be represented as $\breve{\mathbf{H}}(s;\vartheta) \in \mathbb{C}^{P\times P}$, where s is the Laplace variable and the number of ports is $P = 2$. A closed-form expression is here used to calculate $\breve{\mathbf{H}}(s;\vartheta)$, but the examples of Sec. VII will base model extraction from a set of samples of the scattering response, available from full-wave electromagnetic solvers.

Manuscript received ...; revised ...

S. Grivet-Talocia and R. Trinchero are with the Department of Electronics and Telecommunications, Politecnico di Torino, Torino 10129, Italy (e-mail: stefano.grivet@polito.it, riccardo.trinchero@polito.it).

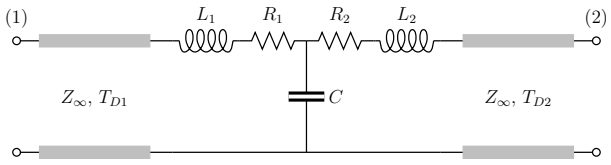

Fig. 1: Transmission line ($Z_\infty = 40\,\Omega$), with an internal lumped discontinuity. Nominal parameters: $L_1 = L_2 = 0.1\,\text{nH}$, $R_1 = R_2 = 1\,\Omega$, $T_{D1} = 100\,\text{ps}$, $T_{D2} = 230\,\text{ps}$. The capacitance C is a free parameter.

The main objective of this paper is to construct a black-box parameterized SPICE equivalent circuit whose input-output scattering response approximates $\breve{\mathbf{H}}(s;\vartheta) \in \mathbb{C}^{P\times P}$ over a prescribed frequency band $[f_{\min}, f_{\max}]$ and parameter domain $\vartheta \in \Theta$. The proposed workflow includes the following steps:

1) choose an appropriate model structure (Sec. III);
2) determine model coefficients (Sec. IV);
3) enforce model stability and passivity (Sec. V);
4) synthesize SPICE netlist (Sec. VI).

III. Model structure

Many different structures may be considered to approximate the true system response in a form that enables a parameterized SPICE netlist synthesis. Following [5], [6], [8], [10], [11], we adopt the so-called *Generalized Sanathanan-Koerner (GSK) form*

$$\mathbf{H}(s;\vartheta) = \frac{\mathbf{N}(s,\vartheta)}{\mathsf{D}(s,\vartheta)} = \frac{\sum_{n=0}^{\bar{n}}\sum_{\ell=1}^{\bar{\ell}} \mathbf{R}_{n,\ell}\,\xi_\ell(\vartheta)\,\varphi_n(s)}{\sum_{n=0}^{\bar{n}}\sum_{\ell=1}^{\bar{\ell}} r_{n,\ell}\,\xi_\ell(\vartheta)\,\varphi_n(s)}, \quad (1)$$

where $\mathbf{R}_{n,\ell} \in \mathbb{R}^{P\times P}$ and $r_{n,\ell} \in \mathbb{R}$ are the model coefficients, and where $\varphi_n(s)$, $\xi_\ell(\vartheta)$ are suitable basis functions representing the dependence of model numerator and denominator on frequency and parameters, respectively. Note that $\ell = (\ell_1, \ldots, \ell_\rho)$ is a multi-index when the parameter domain $\Theta \subset \mathbb{R}^\rho$.

We use the partial fraction basis functions for frequency, e.g., $\varphi_0(s) = 1$ and $\varphi_n(s) = (s - q_n)^{-1}$ for $n > 0$, where q_n are predefined stable "basis poles", either real or in complex conjugate pairs[1]. This choice has become a standard since the introduction of the well-known Vector Fitting scheme [13]. Further, we adopt the system of first-kind Chebychev orthogonal polynomials as parameter-dependent basis functions $\xi_\ell(\vartheta)$, due to their intrinsic normalization and excellent numerical stability properties. If $\rho > 1$, individual Chebychev polynomial bases are used for each dimension in the parameter space.

We remark that the proposed GSK model structure

1) provides a frequency-domain rational approximation of the true scattering matrix;
2) provides a full parameterization of both model poles and model residues: note that we avoid an explicit parameterization of the poles, since their dependence on ϑ may be non-smooth, as outlined in [11];
3) can be realized in a state-space form with parameterized matrices $\{\mathbf{A}(\vartheta), \mathbf{B}(\vartheta), \mathbf{C}(\vartheta), \mathbf{D}(\vartheta)\}$. Although this is a standard approach enabling a subsequent SPICE synthesis, we will avoid constructing such realization, since the parameter dependence of the state-space matrices may be non-smooth. The proposed SPICE synthesis will be detailed in Sec. VI.

[1] If $q_{n+1} = q_n^*$ form a conjugate pair, the corresponding basis functions are redefined as $\tilde{\varphi}_n(s) = \varphi_n(s) + \varphi_{n+1}(s)$ and $\tilde{\varphi}_{n+1}(s) = \mathrm{j}\varphi_n(s) - \mathrm{j}\varphi_{n+1}(s)$ to ensure a real-valued impulse response, see [12], [13].

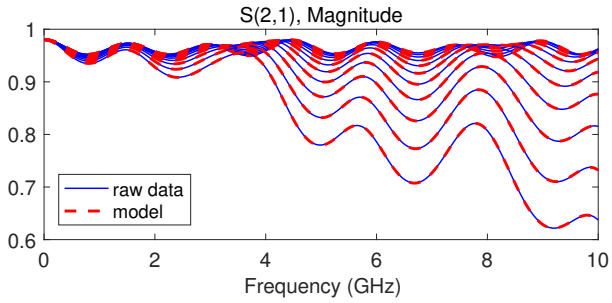

Fig. 2: Comparison between model and raw data for the transmission-line example of Fig. 1.

IV. Model identification

The denomination of model structure as *GSK* is justified by the identification algorithm that is ideally suitable for the determination of the model coefficients, namely the Generalized Sanathanan-Koerner iteration [5], [12], [14]. We start from a set of scattering response samples

$$\breve{\mathbf{H}}_{k,m} = \breve{\mathbf{H}}(\mathrm{j}2\pi f_k; \vartheta_m), \quad k = 1, \ldots, \bar{k},\ m = 1, \ldots, \bar{m}. \quad (2)$$

at discrete frequencies f_k and parameter values ϑ_m, computed by a full-wave solver running a parameter sweep. Then, we set up the following GSK iterative scheme for $\mu = 1, 2, \ldots$

$$\min \left\| \frac{\mathbf{N}^\mu(\mathrm{j}2\pi f_k, \vartheta_m) - \mathsf{D}^\mu(\mathrm{j}2\pi f_k, \vartheta_m)\,\breve{\mathbf{H}}_{k,m}}{\mathsf{D}^{\mu-1}(\mathrm{j}2\pi f_k, \vartheta_m)} \right\|_F^2 \quad (3)$$

where minimization is performed over the model coefficient estimates $\mathbf{R}_{n,\ell}^\mu$ and $r_{n,\ell}^\mu$ at the μ-th iteration. The cost function adopted in (3) is the Frobenius norm of its $P \times P$ matrix argument. The minimization (3) thus corresponds to a simple weighted linear least squares problem, whose solution is achieved through basic pseudoinverse techniques. The iteration is initialized with $\mathsf{D}^0 = 1$ and is stopped when the estimates of the coefficients and the value of the cost function (3) stabilize. See [15], [16] for a discussion on convergence.

Running the GSK iteration on the transmission-line example of Fig. 1 leads to the results depicted in Fig. 2, where the model responses are compared to the nominal (exact) responses over the modeling bandwidth $[0, 10]\,\text{GHz}$. Here, $\bar{m} = 10$ parameter samples and $\bar{k} = 1000$ frequency samples were used, with a rational model order $\bar{n} = 18$ and first-order ($\bar{\ell} = 2$) Chebychev polynomial bases. These orders were adapted to achieve a worst-case RMS fitting error less than 10^{-3} among all scattering responses.

V. Stability and passivity enforcement

Our main objective is a parameterized SPICE equivalent that can be used in transient analyses without incurring in unstable behaviors. It is well-known that such instabilities can be avoided by ensuring the passivity of the model [17], [18]. For the adopted scattering representation, the model transfer function $\mathbf{H}(s;\vartheta)$ must be Bounded Real (BR) [19], [20] throughout the parameter space $\vartheta \in \Theta$, i.e.

1) $\mathbf{H}(s;\vartheta)$ regular for $\mathrm{Re}\{s\} > 0$,
2) $\mathbf{H}^*(s;\vartheta) = \mathbf{H}(s^*;\vartheta)$,
3) $\mathbf{I}_P - \mathbf{H}^{\mathsf{H}}(s;\vartheta)\mathbf{H}(s;\vartheta) \geq 0$ for $\mathrm{Re}\{s\} > 0$,

where $^{\mathsf{H}}$ is the Hermitian transpose, and $\mathbf{I}_P$ is the identity matrix of size P. Whereas condition 2 is automatically verified by the adopted model structure (1), we address condition 1 (related to stability) and condition 3 (passivity) separately.

A. Uniform stability

The BR condition 1 is guaranteed when all model poles have a strictly negative real part throughout the parameter space

$$\mathrm{Re}\{p_n(\vartheta)\} < 0 \quad \forall \vartheta \in \Theta,\ n = 1, \ldots, \bar{n}, \tag{4}$$

where $p_n(\vartheta)$ are the parameter-dependent zeros of the model denominator, such that $\mathsf{D}(p_n(\vartheta),\vartheta) = 0$. As already noted, each $p_n(\vartheta)$ may have a non-smooth dependence on ϑ, therefore a direct enforcement of (4) is problematic.

Let us focus on the scalar model denominator $\mathsf{D}(s,\vartheta)$, which may be considered as a separate parameter-dependent one-port dynamical system, whose definition in (1) provides its explicit pole-residue expansion. The poles are the basis poles q_n, with corresponding residues

$$r_n(\vartheta) = \sum_{\ell=1}^{\bar{\ell}} r_{n,\ell}\, \xi_\ell(\vartheta). \tag{5}$$

We see that

- $\mathsf{D}(s,\vartheta)$ is regular for $\mathrm{Re}\{s\} > 0$, since the basis poles q_n are stable by assumption;
- $\mathsf{D}^*(s,\vartheta) = \mathsf{D}(s^*,\vartheta)$ by construction;

If we are able to enforce the additional constraint

$$\mathrm{Re}\{\mathsf{D}(s,\vartheta)\} \geq 0 \quad \text{for} \quad \mathrm{Re}\{s\} > 0, \quad \forall \vartheta \in \Theta \tag{6}$$

then $\mathsf{D}(s,\vartheta)$ will be Positive Real (PR) [19], [20] (a passive immittance function) throughout the parameter space. Considering now that [12], [19]

- if $\mathsf{D}(s,\vartheta)$ is PR, then also $\mathsf{D}^{-1}(s,\vartheta)$ is PR (if it exists),
- any PR system is stable since regular for $\mathrm{Re}\{s\} > 0$,

we conclude that enforcing (6) is a sufficient condition to guarantee that the poles of $\mathsf{D}^{-1}(s,\vartheta)$, equivalently, the zeros $p_n(\vartheta)$ of $\mathsf{D}(s,\vartheta)$ are stable, as required in (4).

A set of algebraic PR constraints for the denominator are obtained by sampling (6) at suitable frequency $\hat{f}_k$ and parameter $\hat{\vartheta}_m$ values, as

$$\mathrm{Re}\left\{ \sum_{n=0}^{\bar{n}} \sum_{\ell=1}^{\bar{\ell}} r_{n,\ell}\, \xi_\ell(\hat{\vartheta}_m)\, \varphi_n(\mathrm{j}2\pi\hat{f}_k) \right\} \geq 0. \tag{7}$$

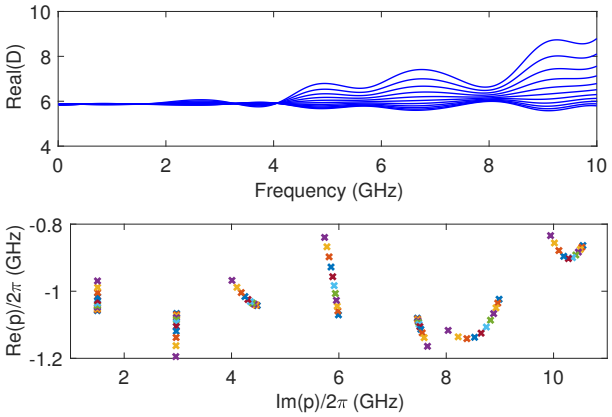

Fig. 3: Top panel: real part of the denominator submodel $\mathsf{D}(s,\vartheta)$ for the transmission-line example of Fig. 1; bottom panel: model poles (zoom) computed over a fine parameter sweep (different colors correspond to different parameter values).

Embedding these constraints into (3) provides a linear least squares problem with linear inequality constraints for each GSK iteration. This is a convex optimization problem, which is readily solved through, e.g., interior point schemes [21]. The strategy for the determination of the frequency $\hat{f}_k$ and parameter samples $\hat{\vartheta}_m$ should be adaptive in order to minimize the number of constraints. The Reader is referred to the guidelines discussed in [22], see also [12], [23], [24].

The top panel of Fig. 3 depicts the real part of the denominator submodel $\mathsf{D}(s,\vartheta)$, comfirming that this denominator is uniformly PR throughout the parameter range. Consequently, all model poles are expected to have a negative real part. This is confirmed by the bottom panel of Fig. 3, which displays the model poles (denominator zeros) over a fine sweep of the parameter (only part of the poles are displayed for clarity, but the maximum real part among all parameterized poles is $\max_{n,\vartheta}\{\mathrm{Re}\{p_n(\vartheta)/2\pi\}\} = -0.83\,\mathrm{GHz} < 0$). This figure also confirms the capability of proposed model structure to effectively represent (implicitly) model poles that are parameter-dependent.

As a final remark, we note that when (6) is verified, then $\mathsf{D}(s,\vartheta)$ and $\mathsf{D}^{-1}(s,\vartheta)$ can be considered as the two immittances (admittance and impedance or viceversa) of a passive one-port. This fact will be useful for the SPICE synthesis discussed in Sec. VI.

B. Uniform passivity

We focus now on the passivity of the parameterized GSK model, expressed by condition 3 in Sec. V. It is well known [12] that this condition is equivalent to requiring that the maximum singular value $\sigma_{\max}$ of the scattering matrix is unitary bounded at all frequencies

$$\sigma_{\max}\{\mathbf{H}(\mathrm{j}\omega;\vartheta)\} \leq 1, \quad \forall \omega \in \mathbb{R}, \tag{8}$$

a condition that we must enforce throughout the parameter space $\vartheta \in \Theta$. Let us assume that (8) is violated at some point

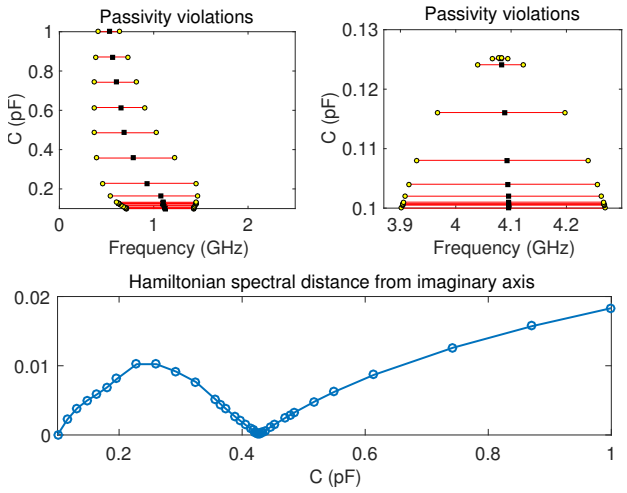

Fig. 4: Top panels: localized passivity violations of the transmission-line model before passivity enforcement; bottom panel: normalized spectral distance $\psi(\vartheta)$ of parameterized Hamiltonian eigenvalues from imaginary axis after passivity enforcement (see text for details).

(ω_i, θ_i), so that the maximum singular value

$$\sigma_{\max}\{\mathbf{H}(\mathrm{j}\omega_i;\vartheta_i)\} = \bar{\sigma}_i > 1 \tag{9}$$

with associated left and right singular vectors $\mathbf{u}_i$, $\mathbf{v}_i$. Define now a model perturbation

$$\widehat{\mathbf{H}}(s;\vartheta) = \mathbf{H}(s;\vartheta) + \Delta\mathbf{H}(s;\vartheta) \tag{10}$$

with

$$\Delta\mathbf{H}(s;\vartheta) = \frac{\sum_{n=0}^{\bar{n}}\sum_{\ell=1}^{\bar{\ell}} \Delta\mathbf{R}_{n,\ell}\,\xi_\ell(\vartheta)\,\varphi_n(s)}{\mathsf{D}(s,\vartheta)} \tag{11}$$

where the denominator $\mathsf{D}(s,\vartheta)$ is left unchanged and the numerator coefficients $\mathbf{R}_{n,\ell}$ are linearly perturbed by $\Delta\mathbf{R}_{n,\ell}$. A first-order singular value perturbation can be applied to $\bar{\sigma}_i$ to enforce its value to be less than one, obtaining the algebraic constraint

$$\mathrm{Re}\left\{\mathbf{u}_i^{\mathsf{H}}\,\Delta\mathbf{H}(\mathrm{j}\bar{\omega}_i;\theta_i)\,\mathbf{v}_i\right\} \le 1 - \bar{\sigma}_i. \tag{12}$$

We see that (12) is also a linear inequality constraint in the coefficient perturbations $\Delta\mathbf{R}_{n,\ell}$. We can then setup an iterative scheme that minimizes model perturbation

$$\min \|\Delta\mathbf{H}(s;\vartheta)\| \tag{13}$$

subject to constraints (12). As for the above-discussed uniform stability enforcement, also these constraints should be determined through and adaptive sampling process, such as the one presented in [22].

The top panel of Fig. 4 depicts two regions in the (ω,ϑ) plane where the transmission-line model results locally non-passive and (8) is violated. The non-passive bands (red lines) are identified by the purely imaginary eigenvalues (yellow dots) of the associated Skew-Hamiltonian/Hamiltonian (SHH) matrix pencil, as discussed in [22], [24]. See the Appendix for a summary of the main SHH properties that are relevant for this work. Black dots are the local singular value maxima σ_i

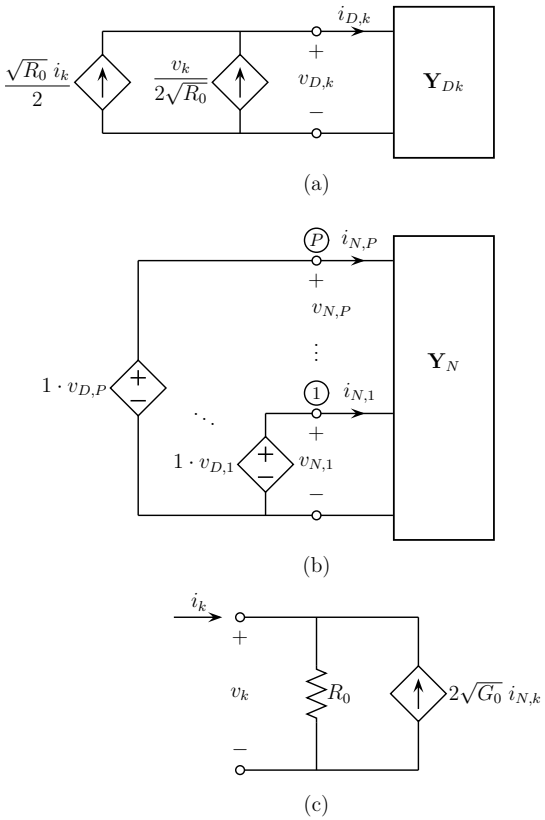

Fig. 5: SPICE realization of (a) denominator submodel (k-th out of P instances); (b) numerator submodel; and (c) external interface of the GSK model (k-th out of P ports, scattering representation, realized in Norton form).

of (9), which are iteratively perturbed until model is passive. Note that $\max_i \sigma_i = 1.00013$, denoting very small passivity violations; such violations are due to the inevitable approximation error involved in the reduced-order model representation. After 5 iterations the model is passive, as confirmed by the bottom panel of Fig. 4, where the parameter-dependent real part of the closest SHH eigenvalues to the imaginary axis $\psi(\vartheta)$ of (24) is depicted as a function of parameter ϑ. Since this distance is uniformly positive, model is uniformly passive [22].

In conclusion, uniform stability and passivity are here achieved through linear inequality constraints applied to separate optimizations of denominator (stability) and numerator (passivity) coefficients.

VI. SPICE SYNTHESIS

We now consider the problem of synthesizing a parameterized GSK model in form (1) into a SPICE netlist. The synthesis strategy that we pursue in the following is dictated by the need of preserving the smooth parameterization of all model coefficients (numerator and denominator), in order to avoid numerical difficulties in SPICE transient runs. To this end, we decompose the model into separate interconnected blocks, as defined below.

1) The denominator submodel is here considered as a one-port with admittance $Y_N(s;\vartheta) = \mathsf{D}(s,\vartheta)$. Therefore,

defining auxiliary (dummy) port voltage and current variables v_D and i_D, respectively, we set

$$i_D = Y_N(s;\vartheta)\, v_D \quad \text{and} \quad v_D = Y_N^{-1}(s;\vartheta)\, i_D. \tag{14}$$

Following the discussion above, this one-port is passive since $Y_N(s;\vartheta)$ is PR, so that the impedance $Z_N(s;\vartheta) = Y_N^{-1}(s;\vartheta) = \mathsf{D}^{-1}(s,\vartheta)$ is guaranteed stable. For later use, we "vectorize" the denominator ports by realizing P separate and identical instances [See Fig. 5(a)] with port voltages $v_{D,k}$ and currents $i_{D,k}$ for $k = 1,\dots,P$, collected in vectors $\mathbf{v}_D, \mathbf{i}_D \in \mathbb{C}^P$. The result can be formally cast as

$$\mathbf{i}_D = \mathbf{D}(s,\vartheta)\, \mathbf{v}_D, \quad \mathbf{v}_D = \mathbf{D}^{-1}(s,\vartheta)\, \mathbf{i}_D, \tag{15}$$

where $\mathbf{D}(s,\vartheta) = \mathrm{diag}\{\mathsf{D}(\mathrm{s},\vartheta)\}$.

2) The numerator submodel is considered as a P-port with admittance matrix $\mathbf{Y}_N(s,\vartheta) = \mathbf{N}(s,\vartheta)$ so that, by defining the auxiliary (dummy) port voltage and current vectors $\mathbf{v}_N, \mathbf{i}_N \in \mathbb{C}^P$, we have

$$\mathbf{i}_N = \mathbf{N}(s,\vartheta)\, \mathbf{v}_N, \tag{16}$$

realized as in Fig. 5(b).

3) The model $\mathbf{H}(s;\vartheta)$ is assumed to be in scattering representation. Therefore,

$$\mathbf{b} = \mathbf{H}(s;\vartheta)\mathbf{a} = \mathbf{N}(s,\vartheta) \cdot \mathbf{D}^{-1}(s,\vartheta) \cdot \mathbf{a}. \tag{17}$$

where $\mathbf{a}, \mathbf{b} \in \mathbb{C}^P$ are the (power-normalized) incident and reflected scattering wave vectors, with components

$$a_k = \frac{1}{2\sqrt{R_0}}(v_k + R_0 i_k), \tag{18}$$

$$b_k = \frac{1}{2\sqrt{R_0}}(v_k - R_0 i_k), \tag{19}$$

where R_0 is the port reference impedance. Interconnection of the various blocks is realized as in Fig. 5 through dependent sources, by setting

- $\mathbf{i}_D = \mathbf{a}$, so that the voltage vector at the output of the denominator block reads $\mathbf{v}_D = \mathbf{D}^{-1}(s,\vartheta)\, \mathbf{a}$. See Fig. 5(a), where a pair of controlled sources are used to synthesize each incident wave a_k;
- $\mathbf{v}_N = \mathbf{v}_D$, so that $\mathbf{i}_N = \mathbf{H}(s;\vartheta)\, \mathbf{a}$, see Fig. 5(b);
- $\mathbf{b} = \mathbf{i}_N$, so that $\mathbf{b} = \mathbf{H}(s;\vartheta)\, \mathbf{a}$. See Fig. 5(c), where a pair of current sources are used to realize the output equation (19) in Norton form.

A. Synthesis of parameterized admittance blocks

The circuit realization of the parameterized admittance blocks corresponding to numerator and denominator is standard [12], [25], except for the novel proposed parameterization scheme. We describe the synthesis of the scalar denominator, since the extension to the matrix numerator case is straightforward. From (1) and (5), we can write

$$i_D = \mathsf{D}(s,\vartheta)\, v_D = \sum_{n=0}^{\bar{n}} j_{D,n} \tag{20}$$

where $j_{D,0} = r_0(\vartheta)\, v_D$ and

$$j_{D,n} = r_n(\vartheta)\, v_{C,n}, \quad \text{with} \quad v_{C,n} = (s - q_n)^{-1}\, v_D \tag{21}$$

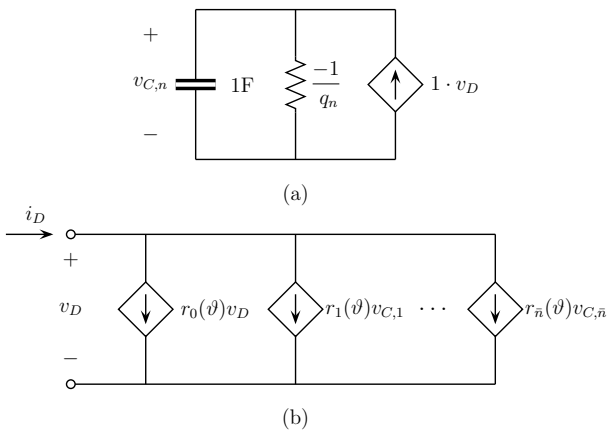

Fig. 6: Synthesis of parameterized admittance block $\mathsf{D}(s,\vartheta)$: (a) elementary RC cell synthesizing the basis pole q_n; (b) external circuit interface.

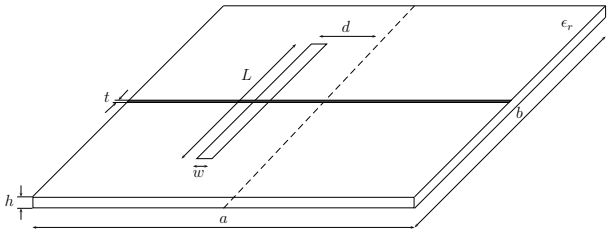

Fig. 7: PCB interconnect over a slotted reference plane ($a = 100\,\mathrm{mm}$, $b = 100\,\mathrm{mm}$, $\epsilon_r = 4.7$, $t = 0.035\,\mathrm{mm}$, $w = 0.12\,\mathrm{mm}$, $h = 0.3\,\mathrm{mm}$). Parameter ranges are $1 \le d \le 25\,(\mathrm{mm})$ and $0 \le L \le 25\,(\mathrm{mm})$.

for $n = 1,\dots,\bar{n}$. Assuming real basis poles $q_n < 0$, each auxiliary voltage $v_{C,n}$ is realized as an elementary RC cell[2], see Fig. 6(a). Each auxiliary current $j_{D,n}$ is realized as a Voltage-Controlled Current Source (VCCS) with a parameter-dependent trans-conductance $r_n(\vartheta)$. Such parameterized VCCS elements are available in most modern SPICE engines (in this work, we use the freeware LTSpice [26]). The superposition (20) of all these currents $j_{D,n}$ is realized as in Fig. 6(b).

To conclude the transmission-line example of Fig. 1, we remark that the model vs data comparison reported in Fig. 2 depicts the results of a double AC and parameter sweep computed form the exported passive model netlist by LTSpice. As expected, this model closely matches the original data.

VII. Examples

A. PCB interconnect over a slotted reference plane

We consider the structure depicted in Fig. 7, consisting of a PCB microstrip running on a reference plane, where a rectangular slot breaks the current return path. The parameters describing the discontinuity are here defined as $\vartheta = (L, d)$, where L is the slot length and d is the slot offset from the midpoint of the microstrip.

[2]Two coupled RC cells can be used to realize a pair of complex conjugate basis poles $q_{n+1} = q_n^*$, see [25].

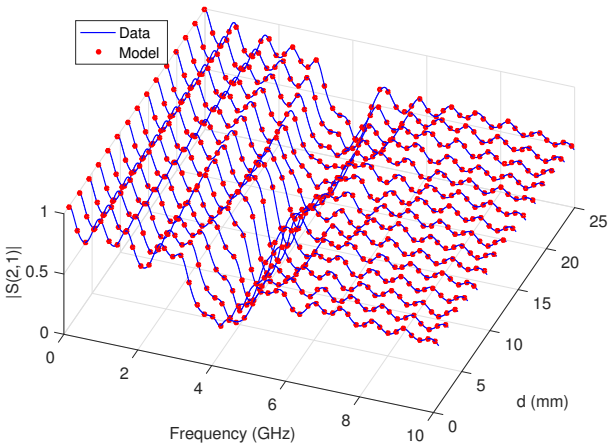

Fig. 8: Validation of the PCB link passive model for $L = 25\,\text{mm}$ and varying d.

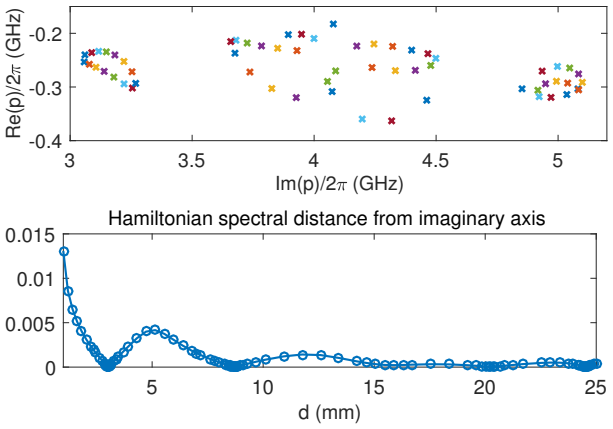

Fig. 9: PCB link passive model ($L = 25\,\text{mm}$ and varying d). Top panel: model poles computed over a sweep on d; bottom panel: Hamiltonian spectral distance $\psi(\vartheta)$ from imaginary axis.

Reference scattering responses ($\bar{k} = 372$ frequency samples and $\{\bar{m}_d = 15, \bar{m}_L = 9\}$ samples for each parameter) were first obtained from a full-wave solver [27], using waveguide port excitations in order to isolate the contribution of the discontinuity. This dataset was then processed by proposed algorithm in order to obtain a passive model with a corresponding parameterized SPICE netlist.

Figure 8 provides a validation of the final passive model vs raw data, considering a fixed slot length $L = 25\,\text{mm}$ while varying the slot offset d (using $\bar{n} = 34$ poles and $\bar{\ell}_N = 10$ and $\bar{\ell}_D = 3$ for numerator and denominator submodels, respectively). Evidence of uniform stability and passivity of the model is provided by the two panels of Fig. 9, where selected model poles over a d parameter sweep are plotted in the top panel, and the Hamiltonian spectral distance $\psi(\vartheta)$ from the imaginary axis after passivity enforcement is depicted in the bottom panel. Figure 10 provides the same validation for the model ($\bar{n} = 29$ and $\bar{l} = 4$ for both numerator and denominator submodels) obtained while keeping a fixed slot offset $d = 25\,\text{mm}$ and varying the slot length L. From Fig. 10, we observe a stopband in the S_{21} response that moves

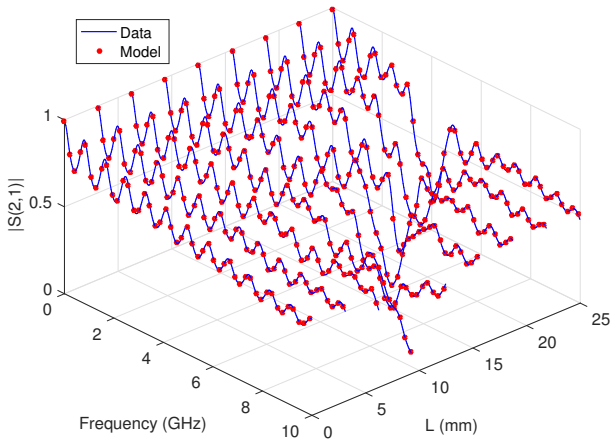

Fig. 10: Validation of the PCB link passive model for $d = 25\,\text{mm}$ and varying L.

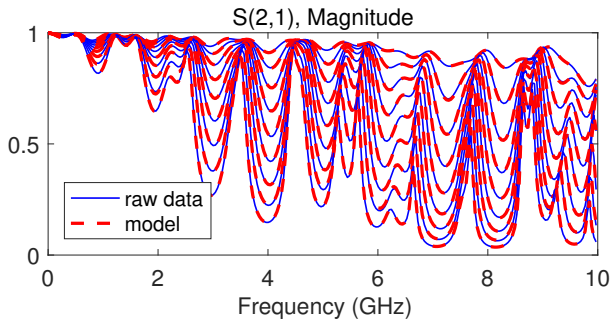

Fig. 11: Validation of the multiboard PCB link passive model for varying via radius a.

towards lower frequencies as L is increased, due to the strong discontinuity that breaks the current return path. This effect is very accurately reproduced by proposed model, throughout the parameter range. The worst-case accuracy in terms of relative RMS error among all frequency/parameter values and scattering responses was below 1%.

B. A via-parameterized multiboard PCB link

This second example is a high-speed signal link (see [28]) running through two PCBs attached by a connector. The signal path is provided by a stripline (total PCB length 14 cm, permittivity $\epsilon_r = 3$ with $\tan\delta = 0.002$) connected by vertical vias located on the two sides of the connector and at the two input/output ports of the link. Each of these vias is surrounded by four ground vias (radius 127 μm and distance from center via 762 μm). All signal vias have a fixed antipad radius $b = 400\,\mu$m, whereas the via radius is considered as a free parameter $a \in [100, 300]\,\mu$m (differently from [22], where the same structure was parameterized by the antipad radius while retaining a fixed via radius). Ports are defined between the first/last vias and the corresponding reference planes across their respective antipads. We remark that signaling on this link is single-ended, with the return current path being formed by the reference PCB planes and by the ground vias. Due to the various link discontinuities, the signal rise/fall times are thus intrinsically lower-bounded, leading to a maximum data rate

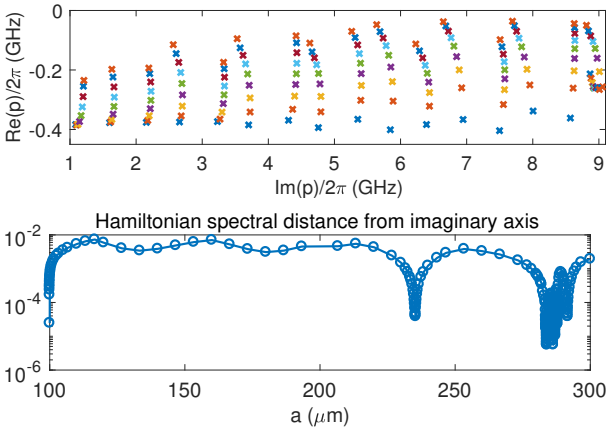

Fig. 12: Multiboard PCB link passive model. Top panel: model poles computed over a sweep on via radius a; bottom panel: Hamiltonian spectral distance $\psi(\vartheta)$ from imaginary axis.

of few Gb/s. Higher data rates would only be possible through differential signaling. Here we consider this single-ended case in order to stress the capability of proposed parameterized modeling algorithm in representing large response variations, as shown below.

A set of sampled scattering responses (Courtesy of Prof. Christian Schuster and Dr. Jan Preibisch, Technische Universität Hamburg-Harburg, Hamburg, Germany) were obtained through a combination of a full-wave field solver (for the connector), lossy transmission-line models for the stripline segments, and a field model for the vias based on [29]. The data for model identification include $\bar{k} = 500$ frequency samples up to 10 GHz for $\bar{m} = 9$ via radius values, linearly spaced within the design range.

Model identification required $\bar{n} = 46$ poles with Chebychev polynomials of degree $\ell_N = 4$ and $\ell_D = 2$ for numerator and denominator submodels, respectively, in order to achieve a fitting accuracy (worst-case relative RMS error) less than 1%. As for previous examples, we report in Fig. 11 a model vs data comparison, showing the very large sensitivity of the insertion loss S_{21} response on the selected parameter. The top panel of Fig. 12 reports the parameterized model poles over a sweep on via radius within its range, confirming uniform model stability. The bottom panel of Fig. 12 shows instead the Hamiltonian spectral distance $\psi(\vartheta)$ from the imaginary axis after passivity enforcement, which confirms that the model is passive.

C. Parameric transient analysis

In order to illustrate the possible application scenarios for proposed modeling approach, we consider again the model discussed in Sec. VII-B, for which we extracted a parametric SPICE netlist, as detailed in Sec. VI. The first simulation setting we consider is a transient pulse distortion analysis under parametric variations (of the via radius). A linear Thévenin source with $R_s = 50\,\Omega$ internal resistance excites a single pulse (100 ps rise/fall time and duration 500 ps). The pulse is received at the far end by a RC load ($R_L = 5\,k\Omega$, $C = 1$ pF), protected by a diode-based clipping circuit limiting the load

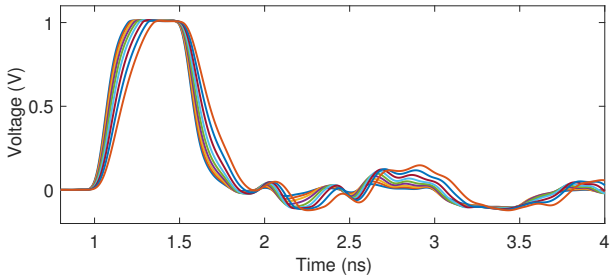

Fig. 13: Transient SPICE simulation of the via-parameterized PCB macromodel with nonlinear terminations (see text).

voltage to $-0.1 < v_L < 1$ V. A parametric sweep is run in SPICE [26] by instantiating the model for different values of the via radius $a \in [100, 300]\,\mu$m, obtaining the results depicted in Fig. 13. We see that the rise time of the received pulse is significantly affected. Also, the reflections induced by the nonlinear load exploit different dynamics as the via radius is changed. The full parametric sweep required a runtime of 3.4 s on a standard laptop.

A second simulation setting is now considered by replacing the driver with a pseudo-random bit generator (bit time 600 ps, rise- and fall-time of 200 ps, internal resistance $R_s = 50\,\Omega$), and the far end termination with a RC load ($R_L = 10\,k\Omega$, $C = 3$ pF) protected by a clipping circuit which limits the load voltage $0 < v_L < 1$ V. A parametric eye diagram simulation was setup in SPICE. The results are shown in Fig. 14 for three different parameter configurations (min, mean, max). The vertical and horizontal eye openings are instead depicted as functions of the via radius in Fig. 15. This analysis confirms the high sensitivity of the transient responses on the considered parameter, which effectively creates a large impedance discontinuity along the transmission path. The time required for computing a full parametric sweep (9 parameter values, 1000 bits) on the eye diagrams was 81 s.

Overall, these results confirm that the proposed modeling approach leads to fast, scalable and accurate models, which can be executed as black-box behavioral circuits as part of those more complex transient analyses required in Signal and Power Integrity assessment.

VIII. Conclusions

This paper proposed a complete workflow for the extraction of behavioral, reduced-order macromodels of wired interconnect links. The model extraction is based on a set of scattering responses of the structure, computed by a field solver for different configurations, as defined by the variation of some geometrical parameter related to internal discontinuities, such as slots in reference planes or via radii. The proposed modeling flow produces a guaranteed stable and passive SPICE netlist, which embeds the dependence of the selected parameters in closed form. As a result, the models can be safely used in time-domain circuit simulations within what-if, optimization and design centering loops.

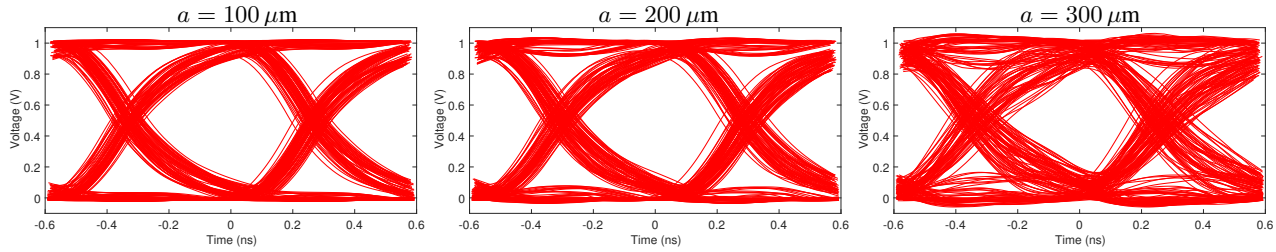

Fig. 14: Eye diagram simulations of the multiboard PCB for three different configurations of the via radius a.

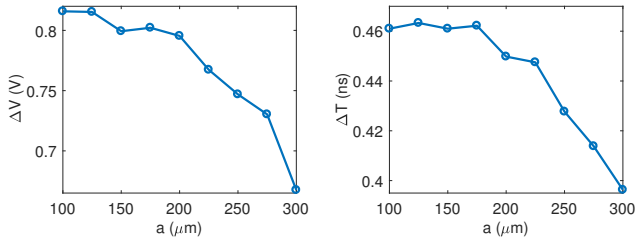

Fig. 15: Vertical (left panel) and horizontal (right panel) eye openings as functions of the parameter a.

IX. Acknowledgements

The Authors are grateful to Prof. Christian Schuster and Dr. Jan Preibisch (Technische Universität Hamburg-Harburg, Hamburg, Germany) for sharing the via-parameterized multiboard PCB link data, and to Dr. Claudio Siviero (Politecnico di Torino) for his support in transient simulations.

Appendix

We briefly recall some known results about Skew-Hamiltonian/Hamiltonian (SHH) pencils and their relation to the passivity of the underlying (parameterized) descriptor systems. Any system in form (1) can be cast as a descriptor system with parameter-dependent generalized state-space matrices $\{\mathbf{E}(\vartheta), \mathbf{A}(\vartheta), \mathbf{B}(\vartheta), \mathbf{C}(\vartheta)\}$ and associated transfer function

$$\mathbf{H}(s;\vartheta) = \mathbf{C}(\vartheta)(s\mathbf{E} - \mathbf{A}(\vartheta))^{-1}\mathbf{B}. \tag{22}$$

Details are reported in [5], [22]. This (scattering) transfer function is BR (passive) for a given value of ϑ when it is asymptotically stable, and when the set of finite purely imaginary eigenvalues of the SHH pencil $(\mathbf{M}(\vartheta), \mathbf{K})$ with

$$\mathbf{M}(\vartheta) = \begin{bmatrix} \mathbf{A}(\vartheta) & \mathbf{B}\mathbf{B}^{\mathsf{T}} \\ -\mathbf{C}^{\mathsf{T}}(\vartheta)\mathbf{C}(\vartheta) & -\mathbf{A}^{\mathsf{T}}(\vartheta) \end{bmatrix}, \quad \mathbf{K} = \begin{bmatrix} \mathbf{E} & \mathbf{0} \\ \mathbf{0} & \mathbf{E}^{\mathsf{T}} \end{bmatrix} \tag{23}$$

is empty, see [12], [24], under the condition that the maximum singular value of $\mathbf{H}(\mathrm{j}\omega;\vartheta)$ is less than one at least at one frequency point. In order to check uniform passivity for $\vartheta \in \Theta$, we define the normalized spectral distance of Hamiltonian eigenvalues from the imaginary axis

$$\psi(\vartheta) = \min_{\lambda(\vartheta)\in\Lambda(\vartheta)} \frac{|\operatorname{Re}\{\lambda(\vartheta)\}|}{\rho(\vartheta)} \tag{24}$$

where $\rho(\vartheta)$ is the spectral radius of the SHH pencil (23), computed considering only the finite eigenvalues. The model is uniformly passive when $\psi(\vartheta) \geq 0$ for all ϑ.

References

[1] S. H. Hall, H. L. Heck, *Advanced Signal Integrity for High-Speed Digital Designs*, John Wiley and Sons, NY, 2009.

[2] C. R. Paul, *Analysis of Multiconductor Transmission Lines*, John Wiley and Sons, NY, 1994.

[3] M. Swaminathan, D. Chung, S. Grivet-Talocia, K. Bharath, V. Laddha, and J. Xie, "Designing and modeling for power integrity," *IEEE Trans. EMC*, vol. 52, pp. 288310, May 2010.

[4] A. Chinea, S. Grivet-Talocia, H. Hu, P. Triverio, D. Kaller, C. Siviero, and M. Kindscher, Signal integrity verification of multichip links using passive channel macromodels, *IEEE Trans. CPMT*, vol. 1, pp. 920933, June 2011

[5] P. Triverio, S. Grivet-Talocia, and M.S. Nakhla, "A Parameterized Macromodeling Strategy with Uniform Stability Test," *IEEE Transactions on Advanced Packaging*, vol. 32, no. 1, pp. 205-215, Feb. 2009.

[6] F. Ferranti, L. Knockaert, T. Dhaene, "Guaranteed Passive Parameterized Admittance-Based Macromodeling," *IEEE Trans. Adv. Packag.*, vol. 33, no. 3, pp. 623–629, Aug. 2010.

[7] S. B. Olivadese, G. Signorini, S. Grivet-Talocia, P. Brenner, "Parameterized and DC-compliant small-signal macromodels of RF circuit blocks," *IEEE Trans. CPMT*, vol. 5, pp. 508-522, April 2015.

[8] E. R. Samuel, L. Knockaert, F. Ferranti, and T. Dhaene, "Guaranteed Passive Parameterized Macromodeling by Using Sylvester State-Space Realizations", *IEEE Trans. MTT*, vol. 61, no. 4, pp. 1444-1454, Mar. 2013.

[9] F. Ferranti, T. Dhaene, and L. Knockaert, "Compact and Passive Parametric Macromodeling Using Reference Macromodels and Positive Interpolation Operators," *IEEE Trans. CPMT*, vol. 2, no. 12, pp. 2080–2088, Dec. 2012.

[10] F. Ferranti, L. Knockaert, and T. Dhaene, "Passivity-Preserving Parametric Macromodeling by Means of Scaled and Shifted State-Space Systems," *IEEE Trans. MTT*, vol. 59, no. 10, pp. 2394–2403, Oct. 2011.

[11] S. Grivet-Talocia and E. Fevola, "Compact Parameterized Black-Box Modeling via Fourier-Rational Approximations," in *IEEE Trans. EMC*, vol. 59, no. 4, pp. 1133-1142, Aug. 2017.

[12] S. Grivet-Talocia and B. Gustavsen, *Passive Macromodeling: Theory and Applications*. New York: John Wiley and Sons, 2016.

[13] B. Gustavsen, A. Semlyen, "Rational approximation of frequency domain responses by vector fitting", *IEEE Trans. Power Del.*, vol. 14, no. 3, pp. 1052-1061, July, 1999.

[14] C. K. Sanathanan and J. Koerner, "Transfer function synthesis as a ratio of two complex polynomials," *IEEE Trans. Automatic Control*, vol. 8, no. 1, pp. 56–58, Jan. 1963.

[15] S. Lefteriu and A. C. Antoulas, "On the Convergence of the Vector-Fitting Algorithm," in *IEEE Trans. MTT*, vol. 61, no. 4, pp. 1435-1443, April 2013.

[16] G. Shi, "On the Nonconvergence of the Vector Fitting Algorithm," in *IEEE Trans. CAS II: Express Briefs*, vol. 63, no. 8, pp. 718-722, Aug. 2016.

[17] P. Triverio, S. Grivet-Talocia, M.S. Nakhla, F. Canavero, R. Achar, "Stability, causality, and passivity in electrical interconnect models", *IEEE Trans. on Advanced Packaging*, vol. 30, no. 4, pp. 795-808, 2007.

[18] S. Grivet-Talocia, "On driving non-passive macromodels to instability," *International Journal of Circuit Theory And Applications*, vol. 37, pp. 863886, Oct 2009.

[19] M. R. Wohlers. *Lumped and Distributed Passive Networks*. Academic press, 1969.

[20] B. D. O. Anderson and S. Vongpanitlerd. *Network analysis and syntesis*. Prentice-Hall, 1973.

[21] S. P. Boyd and L. Vandenberghe. *Convex optimization*. Cambridge Univ Pr, 2004.

[22] S. Grivet-Talocia, "A Perturbation Scheme for Passivity Verification and Enforcement of Parameterized Macromodels", to appear in *IEEE Trans. CPMT*, 2017. Available online: https://arxiv.org/pdf/1706.06395.pdf
[23] S. Boyd, V. Balakrishnan, P. Kabamba, "A bisection method for computing the H_∞ norm of a transfer matrix and related problems", *Math. Control Signals Systems*, Vol. 2, 1989, pp. 207–219.
[24] Z. Zhang and N. Wong, "Passivity Check of S -Parameter Descriptor Systems via S-Parameter Generalized Hamiltonian Methods," in *IEEE Trans. Adv. Packag.*, vol. 33, no. 4, pp. 1034-1042, Nov. 2010.
[25] S. Grivet-Talocia, G. Signorini, S.B. Olivadese, C. Siviero, P. Brenner, "Thermal noise compliant synthesis of linear lumped macromodels", *IEEE Trans. CPMT*, Vol. 5, No. 1, Jan. 2015, pp. 75–85.
[26] LTSPICE IV, *Linear Technology*, available online: www.linear.com
[27] *CST Studio Suite* User's Manual; see also www.cst.com
[28] J. B. Preibisch, T. Reuschel, K. Scharff, J. Balachandran, B. Sen, C. Schuster, "Exploring Efficient Variability-Aware Analysis Method for High-Speed Digital Link Design Using PCE", DesignCon, Jan 31-Feb 2, 2017, Santa Clara (CA), USA.
[29] X. Duan, R. Rimolo-Donadio, H.-D. Brüns, and C. Schuster, "Circular ports in parallel-plate waveguide analysis with isotropic excitations," *IEEE Trans. EMC*, vol. 54, pp. 603612, June 2012.

Stefano Grivet-Talocia (M'98–SM'07) received the Laurea and Ph.D. degrees in electronic engineering from the Politecnico di Torino, Turin, Italy.

From 1994 to 1996, he was with the NASA/Goddard Space Flight Center, Greenbelt, MD, USA. He is currently a Full Professor of electrical engineering with the Politecnico di Torino. He co-founded the academic spinoff company IdemWorks in 2007, serving as the President until its acquisition by CST in 2016. He has authored over 150 journal and conference papers. His current research interests include passive macromodeling of lumped and distributed interconnect structures, model-order reduction, modeling and simulation of fields, circuits, and their interaction, wavelets, time-frequency transforms, and their applications.

Dr. Grivet-Talocia was a co-recipient of the 2007 Best Paper Award of the IEEE TRANSACTIONS ON ADVANCED PACKAGING. He received the IBM Shared University Research Award in 2007, 2008, and 2009. He served as an Associate Editor of the IEEE TRANSACTIONS ON ELECTROMAGNETIC COMPATIBILITY from 1999 to 2001 and as a Guest Editor of the IEEE TRANSACTIONS ON COMPONENTS, PACKAGING AND MANUFACTURING TECHNOLOGY in 2016-2017. He was the General Chair of the 20th and 21st IEEE Workshops on Signal and Power Integrity (SPI2016 and SPI2017).

Riccardo Trinchero (M16) was born in Casale Monferrato, Italy in 1987. He received the M.Sc. and the Ph.D. degrees in Electronics and Communication Engineering from Politecnico di Torino, Torino, Italy, in 2011 and 2015, respectively.

He is currently a Researcher within the EMC Group with the Department of Electronics and Telecommunications at the Politecnico di Torino. His research interests include the analysis of linear time-varying systems, modeling and simulation of switching converters, EMC design and statistical simulation of circuits and systems.